are consistent with Wnt inhibiting β-catenin degradation at, or upstream, of phosphorylation (Fig. 2B, red curve). We can exclude all other points of inhibition. This mode of inhibition predicts that every intermediate downstream of phosphorylation shows the same dip and full recovery. We confirmed this prediction for ubiquitylated β-catenin in cells stimulated with Wnt (Fig. 2, D and E). Thus, partial inhibition of phosphorylation entirely explains the observed dynamics. Full recovery can occur through mass action alone and does not require feedback. Saturation of the destruction complex has been proposed as a mechanism of Wnt action (10), but the dynamics refute this explanation.

To determine how Wnt might affect the individual phosphorylation steps, we applied the same analysis (Fig. 2B). We asked whether Wnt inhibits at or upstream of the priming phosphorylation at S45 by CK1α, or downstream of it, or both. For this analysis, we showed that the majority (80 ± 5%) of CK1α-phosphorylated β-catenin is not phosphorylated by GSK3 (fig. S4). If Wnt only inhibits the GSK3-dependent step, then CK1α-phosphorylated β-catenin should behave similarly to total β-catenin. If Wnt only inhibits the CK1α-dependent step, then CK1α-phosphorylated β-catenin should behave like GSK3-phosphorylated β-catenin. Neither of these occurs. Instead, the accumulation of CK1α-phosphorylated β-catenin is entirely explained by Wnt inhibiting both phosphorylation steps, leading to an initial drop and later accumulation over the initial amount (Fig. 2, B and C). We calculated that the GSK3 and CK1α phosphorylation rates drop in response to Wnt to 24 ± 11% (mean ± SD, $N = 3$) and 16 to 58% (lower/upper bounds) of their initial value, respectively (Fig. 2, F and G) (supplementary materials, section S-IV). Although Wnt might affect the two kinases independently, it seems more likely that Wnt affects a common property of the destruction complex, such as its state of assembly.

It has been suggested that signaling activity may reflect the phosphorylation state, rather than the abundance of β-catenin (15). According to this view, β-catenin not phosphorylated by GSK3, called "active" β-catenin, is the transcriptionally active form (15); without Wnt, it constitutes 1% of cytoplasmic and nuclear β-catenin (16). On addition of Wnt, "active" β-catenin would accumulate massively. For example, a six-fold increase in total β-catenin (Fig. 1B) would translate into a 600-fold increase in "active" β-catenin. Instead, we found that the increase in dephosphorylated β-catenin was comparable to that of total β-catenin (Fig. 3A). Furthermore, in the absence of Wnt, "active" β-catenin was the predominant form (80 ± 5%), as determined by dephosphorylating β-catenin or immunodepleting the GSK3-phosphorylated form (Fig. 3, B and C, and fig. S5). The notion of "active" β-catenin is inconsistent with the observation that almost all β-catenin is unphosphorylated even in the absence of Wnt.

Depictions of signaling pathways have grown exponentially complex with the inclusion of multiple ligands, receptors, extracellular modulators, and downstream targets. Despite this complexity, the core behavior of pathways could be relatively simple. Kinetic analysis of systems, particularly at steady state, provides a powerful strategy to interrogate complex mechanisms; it can provide strong predictions while being insensitive to mechanistic details. In Wnt signaling, β-catenin is subject to a conservation law on the protein flux that permits a few kinetic analyses to resolve long-standing debates about the point of Wnt action. The basic regulatory feature of the pathway is a partial inhibition of two sequential phosphorylation steps without perturbing downstream reactions. Partial inhibition alone establishes the entire dynamics of the β-catenin response. Because a steady state is achieved without saturating the destruction machinery, there in principle can be rapid and facile control of the abundance of β-catenin by tuning its degradation rate through a number of modulators, internal or external to the cell. With a clarification of these central features of the Wnt pathway, we can turn more confidently to its perturbation by drugs and by mutation and to its pathology and pharmacology in different settings.

References and Notes

1. C. H. Schilling, S. Schuster, B. O. Palsson, R. Heinrich, *Biotechnol. Prog.* **15**, 296 (1999).
2. R. Heinrich, T. A. Rapoport, *Eur. J. Biochem.* **42**, 97 (1974).
3. C. Liu et al., *Cell* **108**, 837 (2002).
4. S. Amit et al., *Genes Dev.* **16**, 1066 (2002).
5. M. van Noort, J. Meeldijk, R. van der Zee, O. Destree, H. Clevers, *J. Biol. Chem.* **277**, 17901 (2002).
6. V. F. Taelman et al., *Cell* **143**, 1136 (2010).
7. L. Li et al., *EMBO J.* **18**, 4233 (1999).
8. N. S. Tolwinski et al., *Dev. Cell* **4**, 407 (2003).
9. E. Lee, A. Salic, R. Krüger, R. Heinrich, M. W. Kirschner, *PLoS Biol.* **1**, e10 (2003).
10. V. S. Li et al., *Cell* **149**, 1245 (2012).
11. B. Riggleman, P. Schedl, E. Wieschaus, *Cell* **63**, 549 (1990).
12. F. M. Boisvert et al., *Mol. Cell. Proteomics* **11**, M111.011429 (2012).
13. A. R. Peacocke, *J. Theor. Biol.* **182**, 219 (1996).
14. B. Chance, W. Holmes, J. Higgins, C. M. Connelly, *Nature* **182**, 1190 (1958).
15. F. J. Staal, M. van Noort, G. J. Strous, H. C. Clevers, *EMBO Rep.* **3**, 63 (2002).
16. M. T. Maher, R. Mo, A. S. Flozak, O. N. Peled, C. J. Gottardi, *PLoS ONE* **5**, e10184 (2010).

Tuning the Electronic Absorption of Protein-Embedded All-*trans*-Retinal

Wenjing Wang, Zahra Nossoni, Tetyana Berbasova, Camille T. Watson, Ipek Yapici, Kin Sing Stephen Lee, Chrysoula Vasileiou, James H. Geiger,* Babak Borhan*

Protein-chromophore interactions are a central component of a wide variety of critical biological processes such as color vision and photosynthesis. To understand the fundamental elements that contribute to spectral tuning of a chromophore inside the protein cavity, we redesigned human cellular retinol binding protein II (hCRBPII) to fully encapsulate all-*trans*-retinal and form a covalent bond as a protonated Schiff base. This system, using rational mutagenesis designed to alter the electrostatic environment within the binding pocket of the host protein, enabled regulation of the absorption maximum of the pigment in the range of 425 to 644 nanometers. With only nine point mutations, the hCRBPII mutants induced a systematic shift in the absorption profile of all-*trans*-retinal of more than 200 nanometers across the visible spectrum.

Light-absorbing protein-chromophore complexes play critical roles in a variety of biological processes such as vision, phototaxis, and photosynthesis. The function of these systems depends on the modulation of the spectroscopic properties through protein-chromophore interactions. The rhodopsin family represents a particularly interesting case, where the λ_{max} (absorption maximum) of the same chromophore is modulated from 420 nm (human short wave–sensitive pigment, hSWS) to 587 nm (sensory rhodopsin I) (1, 2). In all cases, a sole chromophore—retinal in its various isomeric forms—is bound via an iminium (also known as a protonated Schiff base, PSB) through the side chain of a lysine residue (3) to various opsins.

Although the mechanism by which rhodopsins alter the absorbance of a single chromophore (the "opsin shift") is still debated, it is generally accepted that wavelength regulation is a result of conformational manipulation of the chromophore and/or directed electrostatics, where the protein

Department of Chemistry, Michigan State University, East Lansing, MI 48824, USA.

*To whom correspondence should be addressed. E-mail: geiger@chemistry.msu.edu (J.H.G.); babak@chemistry.msu.edu (B.B.)

localizes electrostatic potential to various regions of the chromophore [reviewed in (4)]. The latter perturbations lead to stabilization or destabilization of the chromophore's ground and excited states that greatly influence the absorption profile (5–8). Nonetheless, the iminium in all structurally characterized rhodopsins is stabilized, either directly or through a water-mediated network, by a counteranion, which affects the electrostatic environment of the chromophore (9, 10). In contrast, earlier calculations (11) and gas-phase experiments with the retinylidene PSB (12) have indicated that substantial bathochromically shifted spectra would be obtained in a uniformly neutral electrostatic environment in the absence of a PSB counteranion. With the latter principle in mind, we have reengineered proteins capable of binding retinal as a PSB to investigate the details of subtle interactions that can alter the absorption of a bound cationic chromophore. We propose that mutants designed to achieve a more evenly dispersed electrostatic field across the polyene, should lead to "super-red"–absorbing pigments in the absence of a counteranion proximal to the iminium nitrogen.

To systematically study the correlation between structure and absorption wavelength, we selected the intracellular lipid binding protein family (iLBP), and in particular human cellular retinol binding protein II (hCRBPII), as the target for protein engineering (13). Tolerance to mutations and the large binding cavity of iLBPs allow flexibility in the re-design of the protein and enable the binding of a wide range of different ligands (14). The relative rigidity of the iLBP fold makes it an ideal scaffold for protein engineering because it is more likely that mutations will not result in structural rearrangement (14), allowing their specific effects to be compared directly. In addition, we have shown that the chromophore must be fully embedded within the binding pocket, because exposure to the aqueous media would buffer electrostatic changes that result from mutations along the polyene (15). As a result of the latter considerations, hCRBPII was specifically chosen from the iLBP family because it fully encapsulates retinal within its binding cavity.

In prior work, we showed that the correct trajectory of an active-site Lys residue with respect to the electrophilic aldehyde (the Bürgi-Dunitz trajectory) was necessary (16, 17). In that respect, in silico analysis led to the selection of Gln^{108} as the suitable position for the active-site Lys (Fig. 1A). A second mutation, K40L (Fig. 1A), was required because the positively charged Lys residue inhibited the protonation of the Schiff base formed with retinal. Double mutant Q108K:K40L (KL) binds retinal with high affinity (dissociation constant K_d = 29 ± 5 nM) and yields a PSB with λ_{max} = 508 nm, a 68-nm red shift relative to the PSB of retinal with n-butylamine in ethanol (λ_{max} = 440 nm). In contrast to the rhodopsins and our earlier engineered protein systems, and as confirmed by KL's crystal structure, a counteranion for the iminium was purposely and successfully omitted. Alternatively, a putative π-cation interaction with Trp^{106} and the possible interaction with the nearby water network could be stabilizing the protonation of the iminium nitrogen (Fig. 1B).

With KL as the starting point, the electrostatic environment around the chromophore was altered by targeting different zones of the polyene through mutations of nearby amino acids (Fig. 1C). Table 1 illustrates modifications to zones II and III of the bound chromophore. Thr^{51}, Thr^{53}, and Tyr^{19} were targeted, as they were situated relatively close to the polyene (fig. S1). As anticipated, the isosteric replacement of Thr^{51} in zone III (near the iminium) with a hydrophobic amino acid (Val) led to a substantial red shift in absorption, presumably by decreasing the negative polarity near the iminium (Table 1, entry 2; fig. S2). Changes to amino acids in zone II (middle of the chromophore) did not produce red-shifted pigments, highlighted

by mutations of Thr^{53} and Tyr^{19} with a variety of amino acids, which exhibited maximally a 5-nm red shift when replaced with Cys and Trp, respectively (Table 1, entries 3 and 5; table S2). A large bathochromic shift was again observed as a result of the T51V mutation when combined with T53C and/or Y19W (Table 1, entries 4, 6, and 7; figs. S3 and S4). Changes to zone I (ionone ring end) did not correlate well with electrostatic stabilization of a resonating charge (table S3). In fact, unlike the generally accepted postulate that introduction of negative potential around the ionone ring should lead to more red-shifted pigments [reviewed in (8)], introduction of acidic residues in zones I and II resulted in a blue shift (tables S2 and S3). In contrast to the rhodopsins and other engineered systems where a counteranion stabilizes the iminium charge, the present system does not require anionic localization at any point along the polyene because there is no strong ionic interaction at the PSB to counterbalance. The absence of a PSB counteranion yields a conjugated system that is more responsive to subtle changes in its environment, enabling greater bathochromic shift by an overall "softening" (more even distribution) of the electrostatic potential along the polyene.

Further gain in uniformly balancing the electrostatic potential along the polyene came from control of the chromophore's global environment. The estimated dielectric constant inside the binding cavity of proteins (2 to 4) is much lower than that of the aqueous environment (78) (18). Because exposure to the aqueous environment increases the polarization of the electrostatic potential across the chromophore and also dampens the effect of weakly polarized groups to stabilize a resonating cationic charge, we sought to further sequester the binding pocket. Examination of the hCRBPII structure identified Arg^{58}, located in the entrance of the binding pocket, as a potential "leak" that could be capped with a larger, hydrophobic residue. A number of amino acids were substituted for Arg^{58} (table S4); the R58W substitution was the most effective in sequestering the binding pocket from the bulk medium.

Table 1 lists the contribution of the R58W mutation when combined with the KL series of proteins discussed above. A substantial red shift is observed for these mutants, clearly surpassing the absorption of human long wave–sensitive (hLWS) pigment with six overall mutations (590 nm; Table 1, entry 7). Consistent with the idea that solvent exposure can buffer the effect of weakly polarizing amino acids, the R58W-containing series of proteins, which have a more sequestered binding pocket, enhance the red shift of mutations that are introduced far from R58W. For example, T53C and Y19W are ~9 Å from Arg^{58}, yet the R58W mutation yields a much greater red shift when either T53C or Y19W are present (539 nm → 585 nm for T53C; 537 nm → 577 nm for Y19W). As noted, the same two mutations alone led to smaller bathochromic shifts, which suggests that isolating the interior of the protein from the bulk medium greatly enhances the red shift induced by substitutions at positions 53 and
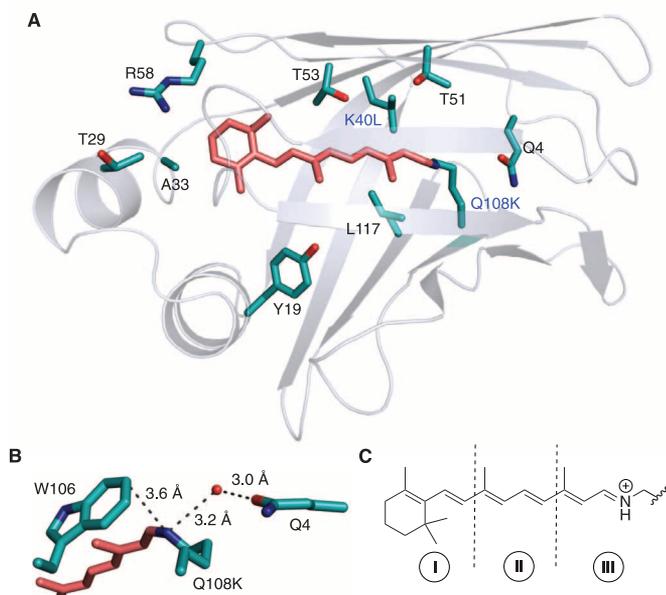

Fig. 1. (A) Crystal structure of Q108K:K40L-hCRBPII, with residues most pertinent to this study highlighted. **(B)** Trp^{106} and a close-lying water molecule hydrogen-bonded to Gln^4 putatively stabilize the protonation of the iminium without the presence of a counteranion. **(C)** Protonated Schiff base of all-trans-retinal. The chromophore is divided into three segments to clarify the discussion of mutations that are close to different locations of the polyene.

Table 1. Q108K:K40L hCRBPII (KL)–based mutants.

Entry	Zone	hCRBPII mutant	λ_{max} (nm) R58	Protein shift*		λ_{max} (nm) R58W	Protein shift†		Enhancement (nm)‡
				(nm)	(cm^{-1})		(nm)	(cm^{-1})	
1	—	KL	508	0	0	527	0	0	—
2	III	KL:T51V	533	25	923	570	43	1431	18 (1.7×)
3	II	KL:T53C	513	5	192	540	13	457	8 (2.6×)
4	II+III	KL:T51V:T53C	539	31	1132	585	58	1881	27 (1.9×)
5	II	KL:Y19W	513	5	192	538	11	388	6 (2.2×)
6	II+III	KL:T51V:Y19W	537	29	1063	577	50	1644	21 (1.7×)
7	II+III	KL:T51V:T53C:Y19W	538	30	1098	590	63	2026	33 (2.1×)

*Protein shift with reference to Q108K:K40L; wavenumbers provide a direct correlation to the change in energy.   †Protein shift with reference to Q108K:K40L:R58W.   ‡Enhancement is calculated as the difference in protein shift between KL-R58W mutants and the KL mutants, and reflects the overall increased red shift in excess of that anticipated from a purely additive effect of R58W. For example, the T51V mutation leads to a 25-nm bathochromic shift (KL versus KL:T51V). A 25-nm red shift would be expected for KL:T51V:R58W versus KL:R58; however, a 43-nm shift is observed. The 18-nm difference in the level of enhancement (factor of 1.7 increase) is a result of the R58W mutation. Numbers in parentheses are relative increases of the protein shift of the KL-R58W mutant series with respect to the KL mutant series.

19. In fact, in all cases, the R58W mutation leads to a factor of ~2 enhancement in red-shifting of the absorption. Although both Cys and Trp can participate in polar interactions, they are also polarizable and could effectively promote conjugation of the positive charge along the polyene in an environment of low dielectric constant.

Inspection of the crystal structures of all available mutants in the PSB region was invaluable to further optimize the binding pocket (representative structure in Fig. 2A). A water network that originates from Thr[1] to Gln[4] and extends to the iminium nitrogen apparently contributes to the stability of the charge on the PSB. Putative disruption of this water network by mutation of Gln[4] in KL-T51V:T53C:Y19W:R58W:T29L to Phe, Trp, Leu, Ala, Asn, and Thr all led to a bathochromic shift from 591 nm up to 610 to 613 nm (table S5). This was akin to removing a polar amino acid residue, such as Thr[51], from zone III. A bathochromic shift was gained with the Q4R mutation (622 nm), presumably as a result of increased positive electrostatic potential in zone III, which further destabilizes the localization of the positive charge on the iminium nitrogen. Evident from the crystal structure of KL-T51V:T53C:Y19W:R58W:T29L:Q4R is the absence of the hydrogen-bonded water network (Fig. 2B). Although the iminium nitrogen is ~6 Å away from the Arg[4] guanidinium, the decreased dielectric constant of the binding pocket translates to higher sensitivity in zone III. Disruption of the putative cation-stabilizing water network was only possible at this late stage of design, having provided the necessary and sufficient means to stabilize the resonating charge along the polyene by earlier mutations. As a point of comparison, the KL:Q4W protein binds retinal to produce a pigment that absorbs maximally at 533 nm, but with a depressed iminium pK_a (8.3 for KL versus 6.2 for KL:Q4W). This is presumably the result of insufficient stabilizing elements, both in the PSB region and along the length of the chromophore.

A final push to gain the most bathochromically shifted pigment focused on further encapsulation of the binding pocket from the aqueous environment. The Ala[33] position, residing on the α helix that functions as a lid for ligand entry, provided a likely candidate (Fig. 2C). A series
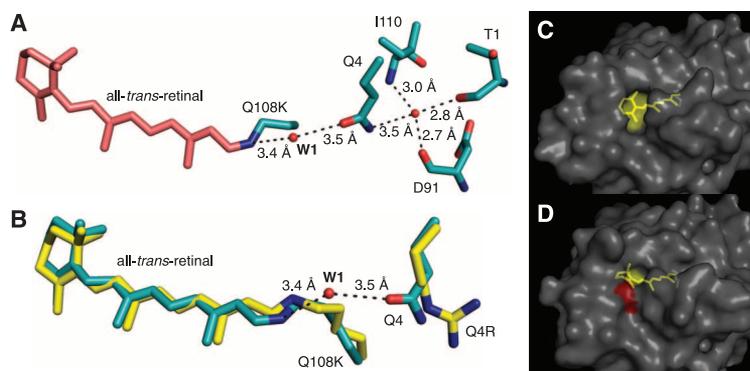

Fig. 2. (A) Crystal structure of Q108K:K40L:T51V:T53C:Y19W:R58W:T29L hCRBPII with Thr[1], Gln[4], Asp[91], and Ile[110] highlighted to show hydrogen bonding to W1, extending to the iminium nitrogen. **(B)** Overlay of the crystal structures of Q108K:K40L:T51V:T53C:Y19W:R58W:T29L hCRBPII (591 nm, cyan structure) and Q108K:K40L:T51V:T53C:Y19W:R58W:T29L:Q4R hCRBPII (622 nm, yellow structure) illustrates that the mutation of Gln[4] results in the loss of the ordered water molecule (**W1**), leading to further bathochromic shift of the retinylidene protein complex. As exemplified in the latter two structures, all mutants that have an ordered water molecule adopt the *cis*-imine geometry. Conversely, *trans*-imine geometry is observed in all Gln[4] mutants without the ordered water molecule. **(C)** Crystal structure of Q108K:K40L:T51V:T53C:Y19W:R58W:T29L hCRBPII (591 nm) illustrates the opening near Ala[33]. **(D)** Crystal structure of Q108K:K40L:T51V:T53C:Y19W:R58W:T29L:A33W hCRBPII (606 nm) shows substantial closing of the orifice (A33W surface shown in red).

of Ala[33] mutants of the KL-T51V:T53C:Y19W: R58W:T29L:Q4F protein were produced (table S6). Incorporation of A33W led to further red-shifting of the absorption (636 nm), likely as a result of sequestering and increasing the polarizability of the binding pocket (Fig. 2D) (19). The nonamutant KL-T51V:T53C:Y19W:R58W:T29L: Q4R:A33W produced the most bathochromically shifted retinylidene-bound protein complex reported thus far, with a λ_{max} of 644 nm (**M11**, Fig. 3). To put this in context, the most red-shifted retinylidene PSB previously observed (measured in vacuum) peaks at 610 nm, whereas 620 nm was considered to be the theoretical maximum (12).

Wavelength regulation toward the most red-shifted hCRBPII mutant (**M11**, 644 nm) showed that removal of the negative polarity in zone III is necessary. Conversely, introduction of negatively polarized residues in this region should result in a blue shift by localizing the cation on the iminium nitrogen. Replacement of Lys[40] with Ser (**M3**, 482 nm) reversed the polarity in zone III and produced a blue-shifted pigment relative to KL. The same was

true for the absorption of Q108K:T51D double mutant, which blue-shifted to 474 nm (**M2**). Further, introduction of L117E (also in zone III) generated the most hypsochromically shifted mutant (**M1**, 425 nm), which is comparable to hSWS pigment.

The ultraviolet-visible (UV-vis) spectra and solutions of a number of hCRBPII mutants bound with retinal are shown in Fig. 3. The figure depicts the regulation of wavelength of a single chromophore, over a 219-nm range, through the redesign of the electrostatic potential of the protein's interior. The hCRBPII mutants not only recapitulate the wavelength regulation observed with the pigmented rhodopsins, but also display red shifts beyond the postulated limit for any retinylidene PSB. These mutants show that extensive wavelength regulation is possible with little contribution from conformational effects. The latter conclusion was based on analysis of crystal structures for this series of mutants that showed little change in the planarity of the chromophore (figs. S6 and S7). As expected, maximal hypsochromicity is achieved by localizing the positive charge on the iminium nitrogen.
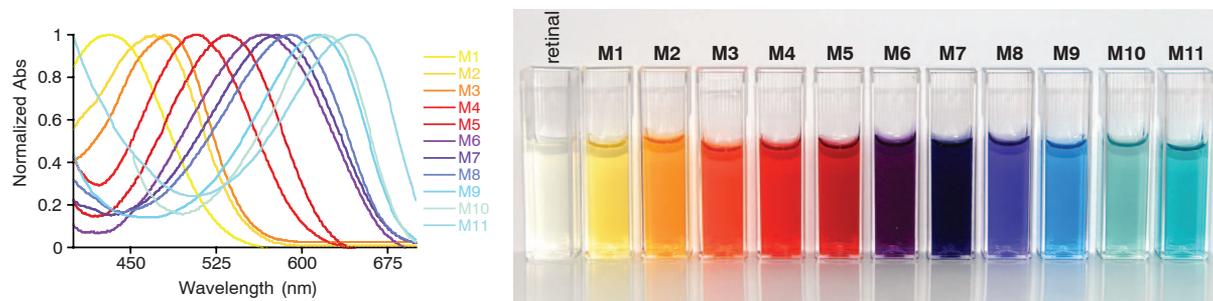
Entry	Pigments	λ_{max} nm	Protein shift nm (cm^{-1})	K_d, nM
1	nBu-retinylidene PSB	440	---	---
2	hSWS	420	-20 (-1,082)	---
M1	Q108K:T51D:L117E	425	-15 (-802)	53±15
M2	Q108K:T51D	474	34 (1,630)	23±6
M3	Q108K:K40S	482	42 (1,980)	28±12
3	sensory rhodopsin II	487	47 (2,193)	---
4	rod-rhodopsin	500	60 (2,727)	---
M4	Q108K:K40L	508	68 (3,042)	29±5
5	hMWS	530	90 (3,859)	---
M5	Q108K:K40L:T51V	533	93 (3,966)	19±7
6	hLWS	560	120 (4,870)	---
7	bacteriorhodopsin	570	130 (5,183)	---
M6	Q108K:K40L:T51V:R58W	570	130 (5,183)	63±4
M7	Q108K:K40L:T51V:Y19W:R58W	577	137 (5,396)	86±6
8	sensory rhodopsin I	587	147 (5,691)	---
M8	Q108K:K40L:T51V:T53C:Y19W:R58W:T29L	591	151 (5,807)	55±5
M9	Q108K:K40L:T51V:T53C:Y19W:R58W:T29L:Q4W	613	173 (6,414)	65±8
M10	Q108K:K40L:T51V:T53C:Y19W:R58W:T29L:Q4R	622	182 (6,650)	70±6
M11	Q108K:K40L:T51V:T53C:Y19W:R58W:T29L:Q4R:A33W	644	204 (7,199)	42±6

Structure inset: all-*trans*-retinal, X = O, λ_{max} = 380 nm; nBu-retinylidene PSB, X = NH-nC$_4$H$_9^{\oplus}$

Fig. 3. Normalized UV-vis spectra of a selected group of hCRBPII mutants (**M1** to **M11**). As indicated in the table, the absorption of the mutants spans from 425 nm (**M1**) to 644 nm (**M11**). For comparison, the wavelengths of various rhodopsins are included. The pigments in the cuvettes were generated by incubation of all-*trans*-retinal (72 μM in 100 mM phosphate buffer, pH 7.3, shown in the left cuvette) with hCRBPII mutants **M1** to **M11** (80 μM protein; the same concentration of retinal was used in all cuvettes). Protein shift is defined as the difference between the absorbance of *n*-butylamine retinylidene PSB and the absorbance of retinal-bound hCRBPII mutants; wavenumbers given in parentheses provide a direct correlation to the change in energy. The binding constants for the hCRBPII mutants (shown as dissociation constants K_d) indicate strong binding of retinal with the proteins.

Extreme bathochromic shifting, on the other hand, depends not on a reversal of polarity but on an even distribution of electrostatic potential across the entire polyene, keeping in mind that a strong interaction of a counteranion to the PSB is not present in these mutants (20). To this end, it is of utmost importance not only to embed the chromophore within the binding pocket, but also to enclose the binding cavity from the bulk medium and distribute the cationic charge evenly along the polyene. Embedding the chromophore enables it to respond to electrostatic perturbations, and this is enhanced by enclosure of the binding pocket. A balanced distribution of the cationic charge across the polyene is generated by evenly distributed neutral electrostatic potential in the binding pocket, leading to "super-red" pigments.

References and Notes

1. K. Palczewski, *J. Biol. Chem.* **287**, 1612 (2012).
2. J. L. Spudich, C. S. Yang, K. H. Jung, E. N. Spudich, *Annu. Rev. Cell Dev. Biol.* **16**, 365 (2000).
3. K. Palczewski, *Annu. Rev. Biochem.* **75**, 743 (2006).
4. M. B. Nielsen, *Chem. Soc. Rev.* **38**, 913 (2009).
5. P. B. Coto, A. Strambi, N. Ferré, M. Olivucci, *Proc. Natl. Acad. Sci. U.S.A.* **103**, 17154 (2006).
6. G. G. Kochendoerfer, S. W. Lin, T. P. Sakmar, R. A. Mathies, *Trends Biochem. Sci.* **24**, 300 (1999).
7. S. W. Lin et al., *J. Biol. Chem.* **273**, 24583 (1998).
8. R. Rajamani, Y. L. Lin, J. Gao, *J. Comput. Chem.* **32**, 854 (2011).
9. T. P. Sakmar, R. R. Franke, H. G. Khorana, *Proc. Natl. Acad. Sci. U.S.A.* **86**, 8309 (1989).
10. T. P. Sakmar, R. R. Franke, H. G. Khorana, *Proc. Natl. Acad. Sci. U.S.A.* **88**, 3079 (1991).
11. B. Honig, A. D. Greenberg, U. Dinur, T. G. Ebrey, *Biochemistry* **15**, 4593 (1976).
12. J. Rajput et al., *Angew. Chem. Int. Ed.* **49**, 1790 (2010).
13. E. Li, A. W. Norris, *Annu. Rev. Nutr.* **16**, 205 (1996).
14. K. Gunasekaran, A. T. Hagler, L. M. Gierasch, *Proteins* **54**, 179 (2004).
15. K. S. S. Lee et al., *ChemPlusChem* **77**, 273 (2012).
16. H. B. Bürgi, J. D. Dunitz, *Acc. Chem. Res.* **16**, 153 (1983).
17. C. Vasileiou et al., *J. Am. Chem. Soc.* **129**, 6140 (2007).
18. J. J. Dwyer et al., *Biophys. J.* **79**, 1610 (2000).
19. Addition of hydroxylamine to two hCRBPII mutants examined the ability to enclose the binding cavity with mutations of Arg[58] and Ala[33]. Reaction of the retinylidene with hydroxylamine would require ready access of the reagent to the PSB. A rapid disappearance of the PSB was observed upon addition of hydroxylamine to the hCRBPII mutant that retained Arg[58] and Ala[33]. Conversely, the protein containing the R58W and A33W mutations resisted change in the presence of hydroxylamine (see supplementary materials for further details).
20. The calculated electrostatic potential of **M10** (622 nm) projected onto the bound retinylidene chromophore is compared to that of **M4** (508 nm) in fig. S5. The comparison shows that to achieve the red shift observed in

M10, the chromophore experiences an even distribution of a neutral electrostatic potential across its length.

Science

AAAS

Tuning the Electronic Absorption of Protein-Embedded All-*trans*-Retinal
Wenjing Wang *et al.*
Science **338**, 1340 (2012);
DOI: 10.1126/science.1226135

This copy is for your personal, non-commercial use only.